The Astrophysical Journal, 824:55 (10pp), 2016 June 10 doi:10.3847/0004-637X/824/1/55

K2-29 b/WASP-152 b: AN ALIGNED AND INFLATED HOT JUPITER IN A YOUNG VISUAL BINARY

A. Santerne[1,2], G. Hébrard[3,4], J. Lillo-Box[5,6], D. J. Armstrong[7,8], S. C. C. Barros[1], O. Demangeon[2], D. Barrado[5], A. Debackere[33], M. Deleuil[2], E. Delgado Mena[1], M. Montalto[1], D. Pollacco[7], H. P. Osborn[7], S. G. Sousa[1], L. Abe[9,33], V. Adibekyan[1], J.-M. Almenara[10,11], P. André[12,33], G. Arlic[33], G. Barthe[33], P. Bendjoya[9,33], R. Behrend[13,33], I. Boisse[2], F. Bouchy[2,13], H. Boussier[14,33], M. Bretton[15,33], D. J. A. Brown[7], B. Carry[9,33], A. Cailleau[33], E. Conseil[16,33], G. Coulon[17,33], B. Courcol[2], B. Dauchet[17,33], J.-C. Dalouzy[33], M. Deldem[18,33], O. Desormières[17,33], P. Dubreuil[33], J.-M. Fehrenbach[12,33], S. Ferratfiat[19,33], R. Girelli[20,21,33], J. Gregorio[22,33], S. Jaecques[33], F. Kugel[23,33], J. Kirk[7], O. Labrevoir[24,33], J.-C. Lachurié[12,33], K. W. F. Lam[7], P. Le Guen[33], P. Martinez[12,33], L. P. A. Maurin[14,33], J. McCormac[7], J-B. Pioppa[25,33], U. Quadri[20,21,26,27,33], A. Rajpurohit[2,28], J. Rey[13], J.-P. Rivet[9,33], R. Roy[29,33], N. C. Santos[1,30], F. Signoret[25,33], L. Strabla[20,21,33], O. Suarez[9,33], D. Toublanc[12,31,33], M. Tsantaki[1], J.-M. Vienney[17,33], P. A. Wilson[3], M. Bachschmidt[33], F. Colas[32,33], O. Gerteis[33], P. Louis[33], J.-C. Mario[33], C. Marlot[33], J. Montier[33], V. Perroud[33], V. Pic[33], D. Romeuf[33], S. Ubaud[33], and D. Verilhac[33]

[1] Instituto de Astrofísica e Ciências do Espaço, Universidade do Porto, CAUP, Rua das Estrelas, 4150-762 Porto, Portugal; alexandre.santerne@astro.up.pt
[2] Aix Marseille Université, CNRS, Laboratoire d'Astrophysique de Marseille UMR 7326, F-13388, Marseille, France
[3] Institut d'Astrophysique de Paris, UMR7095 CNRS, Université Pierre & Marie Curie, 98bis boulevard Arago, F-75014 Paris, France
[4] Observatoire de Haute-Provence, Université d'Aix-Marseille & CNRS, F-04870 Saint Michel l'Observatoire, France
[5] Departamento de Astrofsica, Centro de Astrobiologa (CSIC-INTA), ESAC campus E-28692 Villanueva de la Caada (Madrid), Spain
[6] European Southern Observatory (ESO), Alonso de Cordova 3107, Vitacura, Casilla 19001, Santiago de Chile, Chile
[7] Department of Physics, University of Warwick, Gibbet Hill Road, Coventry CV4 7AL, UK
[8] ARC, School of Mathematics & Physics, Queen's University Belfast, University Road, Belfast BT7 1NN, UK
[9] Laboratoire Lagrange, UMR7239, Université de Nice Sophia-Antipolis, CNRS, Observatoire de la Cote d'Azur, F-06300 Nice, France
[10] Université Grenoble Alpes, IPAG, F-38000 Grenoble, France
[11] CNRS, IPAG, F-38000 Grenoble, France
[12] Observatoire de Belesta-en-Lauragais-Assoc. Astronomie Adagio 30 Route de Revel, F-31450 Varennes, France
[13] Observatoire Astronomique de l'Université de Genève, 51 chemin des Maillettes, 1290 Versoix, Switzerland
[14] SAF—Observatoire, F-84450 St Saturnin les Avignon, France
[15] Observatoire des Baronnies Provencales, Observatoire Astronomique, F-05150, Moydans, France
[16] Observatoire de Géotopia, rue des écoles, F-62350 Mont-Bernenchon, France
[17] Centre d'Astronomie Jean Marc Salomon, association Planète Sciences, 73 rue des Roches, F-77 760 Buthiers, France
[18] Observatoire Les Barres, F-13113 Lamanon, France
[19] Astronomes Amateurs Aixois de l'Observatoire de Vauvenargues, 1185 chemin du Puits d'Auzon, F-13126 Vauvenargues, France
[20] Bassano Bresciano Observatory, Via San Michele,4 I-25020 Bassano Bresciano, Italy
[21] Italian Supernovae Search Project, Italy
[22] Atalaia Group—Crow Observatory, Portalegre, Portugal
[23] Observatoire de Dauban, F-04150 Banon, France
[24] Centre d'Astronomie, Plateau du Moulin á Vent, F-04870, St-Michel-l'Observatoire, France
[25] Groupement Astronomique Populaire de la Région d'Antibes (GAPRA), 2 Rue Marcel-Paul F-06160 Juan-Les-Pins, France
[26] American Association of Variable Star Observers, 49 Bay State Rd., Cambridge, MA 02138, USA
[27] Unione Astrofili Italiani—Sezione Stelle Variabili, Italy
[28] Astronomy and Astrophysics Division, Physical Research Laboratory, Ahmedabad 380009, India
[29] Observatoire de Blauvac, 293 chemin de St Guillaume, F-84570 Blauvac, France
[30] Departamento de Física e Astronomia, Faculdade de Ciências, Universidade do Porto, Rua Campo Alegre, 4169-007 Porto, Portugal
[31] Université de Toulouse, UPS-CNRS, IRAP, 9 Av. colonel Roche, F-31028 Toulouse cedex 4, France
[32] Institut de Mécanique Céleste et Calcul d'Ephémérides—CNRS UMR8028, 77 Av. Denfert-Rochereau, F-75014 Paris, France
[33] European Pro/Am Network of Exoplanetary Transit Observers, France
Received 2016 January 27; accepted 2016 March 20; published 2016 June 10

ABSTRACT

In the present paper we report the discovery of a new hot Jupiter, K2-29 b, first detected by the Super-WASP observatory and then by the *K2* space mission during its campaign 4. The planet has a period of 3.25 days, a mass of $0.73 \pm 0.04\,M_{2\downarrow}$, and a radius of $1.19 \pm 0.02\,R_{2\downarrow}$. The host star is a relatively bright ($V = 12.5$) G7 dwarf with a nearby K5V companion. Based on stellar rotation and the abundance of lithium, we find that the system might be as young as ~450 Myr. The observation of the Rossiter–McLaughlin effect shows that the planet is aligned with respect to the stellar spin. Given the deep transit (20 mmag), the magnitude of the star and the presence of a nearby stellar companion, the planet is a good target for both space- and ground-based transmission spectroscopy, in particular in the near-infrared where both stars are relatively bright.

Key words: planets and satellites: detection – stars: individual (EPIC21189792) – techniques: high angular resolution – techniques: photometric – techniques: radial velocities – techniques: spectroscopic

1. INTRODUCTION

While small exoplanets are currently the most searched-for objects, giant planets are still interesting to characterize for two main reasons: (1) there are still open questions that are not fully understood, such as their formation and their inflation (see Santerne et al. 2016, and references therein) and (2) they are still the best targets for atmosphere characterization from space (e.g., Stevenson et al. 2014) or from the ground (e.g., Croll

Table 1
Various Identification (IDs), Magnitudes, and Coordinates of the Target Star

	Value	Reference
EPIC ID	211089792	Huber et al. (2015)
TYC ID	1818-1428-1	Høg et al. (2000)
WASP ID	152	...
K2 ID	29	...
R.A.	04:10:40.955	Huber et al. (2015)
Decl.	+24:24:07.35	Huber et al. (2015)
pmR.A. (mas yr^{-1})	4.99	Fedorov et al. (2011)
pmDecl. (mas yr^{-1})	−39.73	Fedorov et al. (2011)
Kepler K_p	12.91	Huber et al. (2015)
Johnson B	13.597 ± 0.062	this work
Johnson V	12.526 ± 0.044	this work
2MASS J	10.622 ± 0.035	Cutri et al. (2013)
2MASS H	10.168 ± 0.041	Cutri et al. (2013)
2MASS Ks	10.062 ± 0.034	Cutri et al. (2013)
WISE 3.4 μm	10.095 ± 0.037	Cutri et al. (2013)
WISE 4.6 μm	10.142 ± 0.037	Cutri et al. (2013)
WISE 12 μm	9.991 ± 0.082	Cutri et al. (2013)

et al. 2015). The latter requires planet hosts much brighter than the typical stars targeted by the *CoRoT* (Baglin et al. 2006) and *Kepler* (Borucki et al. 2009) space missions (*V* magnitudes mostly between 14 and 16).

After the failure of two of the reaction wheels, the resurrected *Kepler* mission, *K2* (Howell et al. 2014) is now targeting different fields of view along the ecliptic plane. *K2* targets are proposed by the community through international calls. As a result, *K2* is observing much brighter stars than during the prime mission (*V* magnitudes up to 12) to allow for spectroscopic follow-up and atmosphere characterization, as well as many more M dwarfs (e.g., Almenara et al. 2015; Crossfield et al. 2015).

In this paper we present the discovery of a new giant planet, K2-29 b, transiting a relatively bright ($V = 12.5$) and young (∼450 Myr) star in a visual binary observed during the *K2* campaign 4. In Section 2, we present the target star and the observations, which we then analyze in Section 3. We draw our conclusions and discuss the interest of this new planet in the context of ground-based atmospheric characterization in Section 4.

2. OBSERVATIONS AND DATA REDUCTION

2.1. Ground- and Space-based Photometry

2.1.1. K2 Data

The target star K2-29[34] was observed by the *Kepler* telescope from 2015 February 07 to April 23. Basic information about this target is provided in Table 1. We reduced the *K2* raw pixel data using both the Warwick (Armstrong et al. 2015a, 2015b) and the LAM-*K2* (Barros et al. 2015) pipelines which gave similar results, except that the Warwick light curve has more noise. We therefore adopted the light curve produced by the LAM-*K2* pipeline. A transiting candidate was easily detected by both pipelines as it presents a 2%-deep transit-like event with a periodicity of about 3.258 days. This period is close to 153.5 times the integration time of the long-cadence mode of *Kepler*. This means that the orbital phases covered by *K2* coincide every two periods. As a consequence the transit is poorly sampled by the *K2* data, hence the transit parameters are degenerated and thus they are not precisely determined. To correct for instrumental effects and stellar variability, we normalized the transits by fitting a parabola to 5 hr of out-of-transit data each side of the transit. This reduced light curve is the one used for the analysis described in Section 3. The star also exhibits a clear variability at the level of 1% with a rotation period of about 11 days (see Figure 1). Following the work of McQuillan et al. (2013, 2014), we computed the autocorrelation function of the light curve. We find that the host star has a rotation period of 10.79 ± 0.02 days, which is close to three times the orbit of the planet.

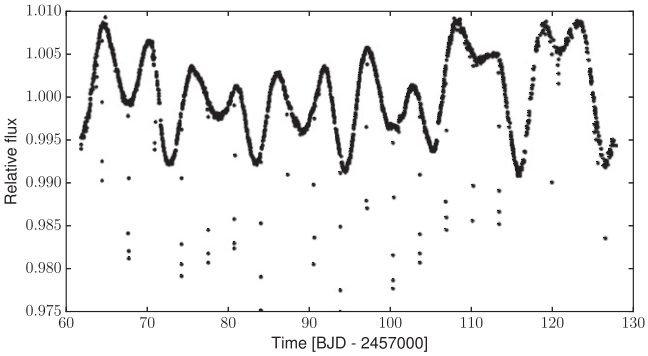

Figure 1. Extracted and detrended *K2* light curve of K2-29.

2.1.2. Archival Super-WASP Data

A 2% transit depth on a star of magnitude 12.5 could be easily detected from the ground. We checked the Super-WASP (Pollacco et al. 2006) public data available in the NASA exoplanet archive 35 and found that the *K2* star K2-29 was observed at least from 2004 July 29 to 2008 March 16. This candidate was found in the WASP data with the same period, but a quick analysis of the spectrum misclassified it as an evolved star, and the star was no longer considered for precise radial velocity follow-up (Super-WASP team 2016, private communication). To allow a comparison of the WASP data with the *K2* data, we converted the heliocentric Julian dates from the WASP data to barycentric Julian dates (BJD) in the barycentric dynamical time (TDB) reference using the online tool kindly provided by Eastman et al. (2010). We then normalized the WASP transits by fitting a parabola in the out-of-transit parts, as for the *K2* transits.

2.1.3. Professional and Amateur Ground-based Photometry

To improve the sampling of the transit and the precision of the ephemeris we performed a photometric campaign to observe the transit that occurred on 2016 January 15 using a network of professional and amateur facilities in Europe (France, Portugal, and Italy). In total 19 observatories detected the same transit and are listed in Table 2. The data were extracted using aperture photometry with the software `Munipack` (Hroch 2014) or `AstroImageJ` (Collins

[34] Guest Observer program GO4007.

[35] http://exoplanetarchive.ipac.caltech.edu

Table 2
List of Photometric Facilities Used to Observe the Transit on 2016 January 15

ID	Observatory/Telescope	Location	UAI Code	Aperture Size	Filter	Observers
3	C2PU	Calern Observatory (FR)	010	1.04 m	r′	LA, JPR, PB, OS
4	ADAGIO	Belesta-en-Lauragais (FR)	⋯	0.82 m	R	PA, JCL, JMF, PM, DT
5	TJMS	Buthiers (FR)	199	0.59 m	R	BD, OD, GC, JMV
6	Centre Astro	St-Michel-l'Observatoire (FR)	⋯	0.58 m	R	OL
7	Baronnies Provencales	Moydans (FR)	B10	0.43 m	R	MB
8	TAC	Calern Observatory (FR)	010	0.40 m	clear	FS, JBP
9	Blauvac	Blauvac (FR)	⋯	0.40 m	clear	RR, RB
10	Géotopia	Mont-Bernenchon (FR)	⋯	0.32 m	clear	EC
11	CROW	Portalegre (PT)	⋯	0.30 m	clear	JG
12	Bassano Bresciano	Bassano Bresciano (IT)	565	0.30 m	clear	UQ, LS, RG
13	AAAOV	Vauvenargues (FR)	⋯	0.30 m	clear	SF
14	⋯	Cuq (FR)	⋯	0.30 m	R	AC, VP
15	Blauvac	Blauvac (FR)	⋯	0.28 m	V	RR, RB
16	⋯	St Saturnin les Avignon (FR)	⋯	0.28 m	R	HB, LM
17	Dauban	Banon (FR)	⋯	0.20 m	r′	FK
18	Les Barres	Lamanon (FR)	K22	0.20 m	clear	MD
19	⋯	Sauternes (FR)	⋯	0.20 m	clear	GA
20	Aspremont	Aspremont (FR)	⋯	0.20 m	clear	PD, GB, SJ
21	⋯	Montebourg (FR)	⋯	0.11 m	R	JCD

Note. The IDs 1 and 2 are for *K*2 and Super-WASP, respectively.

et al. 2016). We converted all the times into BJD TDB and normalized the transits as for the *K*2 and Super-WASP data.

2.2. High-resolution Imaging

2.2.1. FTN Seeing-limited Imaging

The SDSS DR9 (Ahn et al. 2012) images of the star K2-29 revealed the presence of a close companion. To characterize this companion further, we obtained seeing-limited images with the Faulkes Telescope North (FTN), operated by the LCOGT network (Brown et al. 2013). We collected three exposures of 20 s each in the B, V, and R bands. We clearly detected a stellar companion located at about 4.″3 and ≈35° north-to-east (see Figure 2).

We searched for archival data in the Digitalized Sky Survey. Images taken in 1949 and 1993 do not resolve this stellar companion but one can clearly see an elongated point-spread function. The angular separation is about 3″ and 4.″5, with angles of ≈35° and 37° (north-to-east) in the 1949 and 1993 images, respectively. This suggests that star B is a physical companion of star A. In the rest of this paper, we refer to components A and B as the brightest and faintest stars in the system, respectively. Using aperture photometry, we find that component B is fainter than star A by 2.40 ± 0.03 mag, 2.14 ± 0.02 mag, and 1.78 ± 0.01 mag in the B, V, and R bands, respectively. We then used the contaminated magnitudes from the APASS catalog (Munari et al. 2014) to derive the *B* and *V* magnitudes of star A, which are reported in Table 1.

2.2.2. AstraLux Lucky-imaging Observations

To search for other stellar companions in the system we performed high-resolution imaging with the AstraLux lucky-imaging instrument (Hormuth et al. 2008) mounted at the 2.2 m telescope in the Calar Alto Observatory (Spain). We observed this target in the i′ and z′ bands on 2015 November 20 under relatively good weather conditions (seeing of around 0.″9 and fair transparency with about 0.2 mag of extinction at the zenith). We obtained 90,000 frames of 30 ms in full frame mode (24 × 24″) for the i′ band and 57,000 frames of 30 ms for the z′ band. The frames were reduced using the observatory pipeline described in Hormuth et al. (2008). The pipeline performs a basic reduction of the individual frames (bias and flat-field correction), sorts them by image quality in terms of the Strehl ratio (Strehl 1902), then aligns and combines the best 10% of the frames to produce the final near-diffraction limited image. We found no extra star besides star B. We used an image from the M15 globular cluster to obtain the astrometric calibration (see Lillo-Box et al. 2014, for details). In the z′ band image star B is located at 4.307 ± 0.″018. According to our aperture photometry, star B is fainter than star A by 1.59 ± 0.01 mag and 1.42 ± 0.01 mag in the i′ and z′ bands, respectively. The 5σ sensitivity curves of the two images within the first 3″ were then computed by following the prescriptions in Lillo-Box et al. (2014). The result is presented in Figure 2. No additional objects are found within these limits.

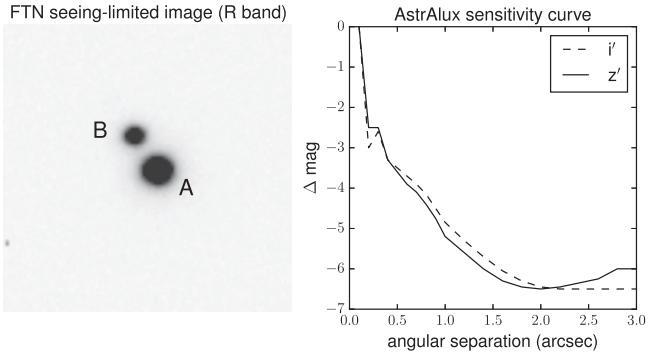

Figure 2. High-resolution imaging of K2-29. Left panel: FTN R-band image (30″ × 30″, north is up, east is right). Right panel: 5-σ sensitivity curve from AstraLux lucky-imaging observations.

Table 3
Radial Velocity Data for the Target Star K2-29 with the Main Spectroscopic Diagnostics

Epoch BJD_{TDB}	RV (km s^{-1})	σ_{RV} (km s^{-1})	BIS (km s^{-1})	σ_{BIS} (km s^{-1})	FWHM (km s^{-1})	σ_{FWHM} (km s^{-1})	Instrument
2457312.54420	32.684	0.021	−0.045	0.042	9.527	0.052	CAFE
2457313.65075	32.827	0.030	−0.013	0.060	9.455	0.075	CAFE
2457351.49132	32.761	0.049	−0.045	0.098	9.411	0.122	CAFE
2457304.63868	32.980	0.006	−0.044	0.012	10.875	0.016	SOPHIE
2457332.61873	32.777	0.009	0.013	0.017	10.935	0.024	SOPHIE
2457364.45580	32.834	0.012	0.002	0.022	10.897	0.031	SOPHIE
2457378.47029	32.820	0.006	−0.019	0.011	10.814	0.015	SOPHIE
2457383.51446	32.907	0.006	−0.015	0.011	11.004	0.015	SOPHIE
2457384.44394	32.792	0.005	−0.019	0.009	10.895	0.013	SOPHIE
2457386.50338	32.968	0.008	−0.026	0.015	10.862	0.020	SOPHIE
2457400.45128	32.802	0.014	−0.041	0.025	10.711	0.035	SOPHIE
2457401.40215	32.843	0.017	−0.011	0.031	10.742	0.043	SOPHIE
2457402.37990	32.983	0.012	−0.026	0.021	10.704	0.029	SOPHIE
2457403.24248	32.900	0.024	−0.013	0.043	10.858	0.059	SOPHIE
2457403.25915	32.895	0.016	−0.011	0.028	10.801	0.039	SOPHIE
2457403.27577	32.882	0.014	−0.044	0.025	10.796	0.035	SOPHIE
2457403.29257	32.871	0.013	−0.031	0.024	10.762	0.034	SOPHIE
2457403.30921	32.872	0.015	−0.032	0.027	10.729	0.038	SOPHIE
2457403.32586	32.889	0.017	−0.007	0.030	10.799	0.041	SOPHIE
2457403.34251	32.885	0.018	0.002	0.032	10.810	0.045	SOPHIE
2457403.35918	32.844	0.016	−0.054	0.029	10.759	0.040	SOPHIE
2457403.37584	32.795	0.017	−0.039	0.030	10.790	0.042	SOPHIE
2457403.39253	32.852	0.016	−0.021	0.028	10.727	0.040	SOPHIE
2457403.40920	32.876	0.019	−0.058	0.033	10.857	0.046	SOPHIE
2457403.42583	32.842	0.020	−0.058	0.036	10.797	0.050	SOPHIE
2457403.44257	32.867	0.024	0.004	0.043	10.848	0.060	SOPHIE
2457403.45919	32.845	0.022	−0.059	0.040	10.825	0.055	SOPHIE
2457404.47376	32.778	0.015	−0.020	0.027	10.822	0.038	SOPHIE
2457405.47099	32.955	0.024	−0.008	0.044	10.700	0.061	SOPHIE
2457392.33082	33.028	0.006	−0.015	0.009	8.218	0.011	HARPS-N
2457393.52070	32.931	0.017	−0.003	0.025	8.338	0.033	HARPS-N
2457393.52923	32.930	0.023	−0.042	0.034	8.317	0.045	HARPS-N
2457393.53642	32.896	0.024	0.064	0.036	8.336	0.047	HARPS-N
2457393.54399	32.936	0.019	0.044	0.029	8.287	0.039	HARPS-N
2457393.55077	32.972	0.016	0.015	0.023	8.196	0.031	HARPS-N
2457393.55803	32.997	0.015	0.036	0.022	8.285	0.030	HARPS-N
2457393.56533	32.947	0.015	0.037	0.023	8.361	0.031	HARPS-N
2457393.57258	32.939	0.014	0.024	0.021	8.329	0.028	HARPS-N
2457393.57980	32.926	0.013	0.024	0.019	8.297	0.026	HARPS-N
2457393.58709	32.915	0.013	0.026	0.020	8.320	0.026	HARPS-N
2457393.59421	32.884	0.013	0.044	0.020	8.317	0.026	HARPS-N
2457393.60151	32.893	0.015	−0.020	0.022	8.282	0.030	HARPS-N
2457393.60869	32.879	0.017	0.070	0.025	8.300	0.033	HARPS-N
2457393.61594	32.871	0.018	0.032	0.027	8.285	0.036	HARPS-N
2457393.62327	32.913	0.019	−0.026	0.029	8.352	0.039	HARPS-N
2457393.63035	32.899	0.022	0.123	0.033	8.322	0.044	HARPS-N
2457393.63752	32.862	0.065	0.044	0.098	8.337	0.131	HARPS-N
2457394.32810	32.840	0.004	0.049	0.007	8.159	0.009	HARPS-N
2457394.51874	32.834	0.014	0.019	0.021	8.171	0.028	HARPS-N
2457395.39857	32.995	0.013	0.032	0.019	8.157	0.025	HARPS-N

2.3. Spectroscopic Follow-up

2.3.1. CAFE

We obtained three observations with the CAFE spectrograph (Aceituno et al. 2013) mounted at the 2.2 m telescope at the Calar Alto Observatory (Spain). CAFE is a high-resolution spectrograph ($R = 63{,}000$) with no movable pieces and a fixed wavelength coverage in the range 4000–9500 Å. Since the spectrograph is not stabilized for temperature and pressure, the ambient conditions of the chamber where the instrument is located are continuously monitored to check for possible changes during the observations. The three spectra were reduced with the observatory pipeline, using the closest ThAr frame to perform the wavelength calibration and master bias and flats for the basic reduction. The radial velocity was extracted by using the cross-correlation technique, using a solar spectrum mask with more than two thousand specifically selected lines (see Lillo-Box

et al. 2015, for details). The radial velocities, bisector, and full width half maximum (FWHM) are provided in the Table 3 together with their uncertainties.

2.3.2. SOPHIE

We observed the target star 27 times with the SOPHIE spectrograph[36] (Bouchy et al. 2013) mounted at the 1.93 m telescope at the Haute-Provence Observatory (France). These observations were carried out from 2015 October 8 to 2016 January 16 as part of a large program to characterize *Kepler* and *K2* candidates. SOPHIE is a fiber-fed high-resolution echelle spectrograph stabilized in temperature and pressure. We used the high-efficiency ($R \sim 40{,}000$) mode which allows about $10\,\mathrm{m\,s^{-1}}$precision in exposure times of less than one hour for this star. We reduced the data using the online pipeline which computes the weighted cross-correlation function (CCF) between the spectra and a numeric mask which corresponds to a G2V star (Baranne et al. 1996; Pepe et al. 2002). The choice of this mask is driven by the spectral type of the host star (see Section 3).

We corrected the data for the charge transfer inefficiency of the CCD (Bouchy et al. 2009) following the procedure described in Santerne et al. (2012). We also corrected the radial velocities from second-order instrumental drifts (not corrected by the wavelength calibration) using the radial velocities from the constant star HD 56124 observed during the same nights, as done in Santerne et al. (2014). We list in Table 3 the radial velocities, bisector, and FWHM of the star with their uncertainties estimated following the methods of Boisse et al. (2010) and Santerne et al. (2015).

Among the 27 observations done with SOPHIE, 16 spectra were collected during the transit night of 2016 January 15 in order to detect the Rossiter–McLaughlin effect.

The fiber of the SOPHIE spectrograph has an aperture on the sky of 3″. Depending on the seeing condition and telescope tracking precision, the light from the component B might have affected the data. If both components are physically bound, it is expected that they have the same center of mass and thus have nearly the same radial velocity. As a consequence, both stars are expected to be unresolved spectroscopically. Using the formalism developed by Santerne et al. (2015), we estimated that in the worst case, i.e., where star B fully contributes to the observed spectrum and both stars have exactly the same systemic radial velocity, and given their difference of magnitudes, the observed radial velocities would be diluted by up to 2%. This is substantially below the radial velocity photon noise we have for individual measurements and thus we concluded that star B should not significantly affect the radial velocities of star A.

2.3.3. HARPS-N

We observed K2-29 with HARPS-N[37], a fiber-fed high-resolution ($R \sim 110{,}000$) echelle spectrograph (Cosentino et al. 2012) mounted on the 3.6 m Telescopio Nazionale Galileo at the La Palma Observatory (Spain). We obtained 22 spectra from 2016 January 4 to 7, among which 19 were collected during the transit night of 2016 January 6 in order to detect the Rossiter–McLaughlin effect. As for SOPHIE, the spectra were reduced using the online pipeline and the radial velocities, bisector, and FWHM were measured on the CCF computed with a G2V mask. The fiber of HARPS-N has an aperture on the sky of 1″ and only star A was observed. The derived radial velocities, bisector, and FWHM are listed in Table 3, together with their uncertainties.

[36] Program IDs: 15B.PNP.HEB.

[37] Program ID: OPT15B_23.

3. MODELING OF THE EXO-PLANETARY SYSTEM

3.1. Spectral Characterization of Stars A and B

The spectral analysis was performed on the co-added HARPS-N spectra of star A. The spectroscopic parameters were derived with the ARES+MOOG method (see Sousa 2014, for details) which is based on the measurement of the equivalent widths of iron lines with ARES (Sousa et al. 2015). This method has been used to derive homogeneous parameters for planet-host stars (e.g., Sousa et al. 2011; Santos et al. 2013). We corrected the log g using the asteroseismic calibration of Mortier et al. (2014). We find that star A has a $T_{\rm eff}$ of 5363 ± 43 K, a log g of $4.49 \pm 0.20\,\mathrm{g\,cm^{-2}}$, a micro-turbulence velocity $\upsilon_{\rm micro}$ of $1.05 \pm 0.08\,\mathrm{km\,s^{-1}}$, and an iron abundance [Fe/H] of 0.16 ± 0.03 dex. Using the method described in Boisse et al. (2010) on the CCF, we find a $\upsilon \sin i_\star$ of $4 \pm 1\,\mathrm{km\,s^{-1}}$. We find evidence of lithium in the co-added spectrum with an abundance of A(Li) $= 1.05 \pm 0.2$ dex.

We attempted to take a spectrum of star B with HARPS-N but the automatic guiding of the telescope was moving to star A. Therefore, to characterize star B, we used the magnitude differences measured by the FTN and AstraLux facilities (see Section 2). We modeled the spectral energy distribution (SED) of both stars using the BT-SETTL atmosphere models (Allard 2014) which we integrated in the B, V, R, i′, and z′ bands. We used the result from the spectral analysis to estimate the magnitudes of star A and we derived the spectroscopic parameters of star B by fitting the observed differences of magnitude through a Markov chain Monte Carlo algorithm (MCMC). We assumed that both stars are at the same distance, and hence have the same interstellar extinction, and that they have the same iron abundance. At each step of the MCMC we checked that the stellar parameters did not correspond to unphysical stars or stars older than the universe, according to the Dartmouth evolution tracks of Dotter et al. (2008). We find that star B has a $T_{\rm eff}$ of 4400 ± 66 K and a log g of $4.60 \pm 0.04\,\mathrm{g\,cm^{-2}}$. This corresponds to a spectral type of K5V according to Cox (2000).

This allows us to determine precisely the contamination of the star B in the light curves of star A. The contaminant fully contributes to the flux measured either by *K2*, WASP, or the other professional and amateur facilities. By integrating the SED models in the *Kepler*, r′, and V bands, we find that the contamination is $15.3 \pm 0.4\%$, $15.4 \pm 0.4\%$, and $12.8 \pm 0.4\%$, respectively.

3.2. Combined Analysis of the System

We analyzed all the light curves, radial velocities[38], and the magnitudes (listed in Table 1) of the target star using `PASTIS` software (Díaz et al. 2014; Santerne et al. 2015). It models the transit light curves using a modified version of the `JKTEBOP` code (Southworth 2011, and references therein) that we

[38] We excluded for this analysis the two transit nights observed by SOPHIE and HARPS-N. By doing this, we avoid biasing the system parameters with possible instrumental systematics. The analysis of the Rossiter–McLaughlin effect is left to the next section.

oversampled by a factor of 10 to compensate the long integration time of the *Kepler* data (Kipping 2010). Radial velocities are modeled with a Keplerian orbit and the SED is modeled with the BT-SETTL library (Allard 2014). Stellar parameters are determined with the Dartmouth stellar evolution tracks and limb darkening coefficients are taken from the theoretical values of Claret & Bloemen (2011).

The statistical analysis of the data was performed with a MCMC algorithm which is fully described in Díaz et al. (2014). The model is described by six free parameters for the star ($T_{\rm eff}$, log g, [Fe/H], the systemic radial velocity υ_0, the distance d, and the interstellar extinction $E(B-V)$), seven free parameters for the transiting planet (period P, epoch of first transit T_0, radial velocity amplitude K, the radius ratio k_r, the orbital eccentricity e, inclination i, and the angle of periastron ω). We added to the model an extra source of white noise (jitter), an out-of-transit flux, and the contamination level for each of the 21 light curves listed in Table 2 which are left free in the analysis. Finally, we also added a jitter term for each of the radial velocity instruments, a radial velocity offset between them, and a jitter term for the SED. In total, the model is composed of 82 free parameters.

We choose uninformative priors as much as possible, except for the stellar parameters that we constrained using on the results of the spectral analysis and the orbital ephemeris to speed up the convergence. We choose a Beta distribution as the prior for the orbital eccentricity (Kipping 2013). The exhaustive list of free parameters and their priors is provided in Table 4.

We ran five exploratory MCMC chains of 10^5 iterations with an initial guess randomly drawn from the joint prior distribution. We then ran 20 MCMC chains of 3×10^5 iterations starting from the best solution found in the exploratory MCMC, to further explore the posterior distribution in the vicinity of the global maximum. All chains converged toward the same solution which is assumed to be the global maximum. We then removed the burn-in phase of each chain before thinning (keep only one sample per maximum correlation length among all the parameters of each chain) and merging them to obtain more than 1000 independent samples of the posterior distribution. We finally determined the median and 68.3% confidence interval for each of the free parameters that we report in Table 4. Note that the uncertainties reported in this table are only the statistical ones and do not take into account the unknown uncertainties on the models.

We display in Figure 3 the phase-folded transit light curves from the 21 different instruments with the best-fit model. In Figure 4, we plot the phase-folded radial velocity data together with the best-fit model and the residuals. The rms of the radial velocity data are 23 m s^{-1}, 12 m s^{-1}, and 10 m s^{-1}, for CAFE, SOPHIE, and HARPS-N, respectively. We find no significant drift in the radial velocity data, with an upper limit of ± 40 m s^{-1} yr^{-1} at the 99% confidence interval.

3.3. Analysis of the Rossiter–McLaughlin Effect

We analyzed the radial velocity data obtained during the transit nights of 2016 January 6 and 15 with HARPS-N and SOPHIE, respectively. To model the Rossiter–McLaughlin effect, we used the formalism developed by Boué et al. (2013). We are neglecting here the effects of convective blueshift and macro-turbulence. We fit the data using the MCMC procedure as described above. We used the results of the combined analysis, listed in Table 4, as the priors for the orbital and transit parameters. We used a uniform prior for the spin–orbit angle λ and assumed a prior for the $\upsilon \sin i_\star$ which follows a normal distribution with a mean of 4 km s^{-1} and a width of 1 km s^{-1}. To account for the different integration times between HARPS-N (10 minutes) and SOPHIE (20 minutes) data, we oversampled the Rossiter–McLaughlin model to 1 minute before binning it back to the actual HARPS-N or SOPHIE cadence. This is similar to what was proposed for photometric transits by Kipping (2010).

Table 4
List of Free Parameters Used in the PASTIS Analysis of the Light Curves, Radial Velocities, and SED with their Associated Prior and Posterior Distributions

Parameter	Prior[a]	Posterior
Orbital parameters		
Orbital period P (day)	$\mathcal{N}(3.25883;\ 1 \times 10^{-5})$	$3.2588321 \pm 1.9 \times 10^{-6}$
Epoch of first transit T_0 ($\rm BJD_{TDB}$)—2450000	$\mathcal{N}(3219.0128;\ 0.001)$	$3219.0095 \pm 2.2 \times 10^{-3}$
Orbital eccentricity e	$\beta(0.867;\ 3.03)$	0.066 ± 0.022
Argument of periastron ω (°)	$\mathcal{U}(0;\ 360)$	132 ± 21
Inclination i (°)	$\mathcal{S}(70;\ 90)$	$86.66^{+0.11}_{-0.08}$
Planetary parameters		
Radial velocity amplitude K (m s^{-1})	$\mathcal{U}(0;\ 1000)$	103.5 ± 5.4
Planet-to-star radius ratio k_r	$\mathcal{U}(0;\ 0.5)$	$0.14188 \pm 6.2 \times 10^{-4}$
Stellar parameters		
Effective temperature $T_{\rm eff}$ (K)	$\mathcal{N}(5363;\ 43)$	5358 ± 38
Surface gravity log g (g cm^{-2})	$\mathcal{N}(4.49;\ 0.20)$	4.540 ± 0.012
Iron abundance [Fe/H] (dex)	$\mathcal{N}(0.16;\ 0.03)$	0.16 ± 0.03
Reddening $E(B-V)$ (mag)	$\mathcal{U}(0;\ 1)$	0.19 ± 0.02
Systemic radial velocity υ_0 (km s^{-1})	$\mathcal{U}(-100,\ 100)$	32.8786 ± 0.0044
Distance to Earth d (pc)	$\mathcal{P}(2;\ 10;\ 1000)$	185 ± 3
Instrumental parameters[b]		
CAFE radial velocity jitter (m s^{-1})	$\mathcal{U}(0;\ 100)$	35 ± 32
SOPHIE radial velocity jitter (m s^{-1})	$\mathcal{U}(0;\ 100)$	12 ± 4
HARPS-N radial velocity jitter (m s^{-1})	$\mathcal{U}(0;\ 100)$	11^{+15}_{-8}
CAFE—SOPHIE radial velocity offset (m s^{-1})	$\mathcal{U}(-1000;\ 1000)$	77 ± 30
HARPS-N—SOPHIE radial velocity offset (m s^{-1})	$\mathcal{U}(-1000;\ 1000)$	-71 ± 10
SED jitter (mag)	$\mathcal{U}(0;\ 1)$	0.027 ± 0.025

Notes. The choice of prior for the orbital eccentricity is described in Kipping (2013).

[a] $\mathcal{N}(\mu;\ \sigma^2)$ is a normal distribution with mean μ and width σ^2, $\mathcal{U}(a;\ b)$ is a uniform distribution between a and b, $\mathcal{S}(a,\ b)$ is a sine distribution between a and b, $\beta(a;\ b)$ is a Beta distribution with parameters a and b, and $\mathcal{P}(n;\ a;\ b)$ is a power-law distribution of exponent n between a and b.

[b] We did not report in this table the out-of-transit flux, jitter, and contamination for each of the 21 light curves we analyzed, as they are not really meaningful. We choose uninformative priors for the two first ones and a normal prior for the latter one, to correspond with the estimated contamination and its uncertainty (see Section 2.2). Note that for ground-based light curves, we assumed a larger prior width (enlarged by a factor of 10 compared with the estimated error), to account for possible under/over-correction of the sky background.

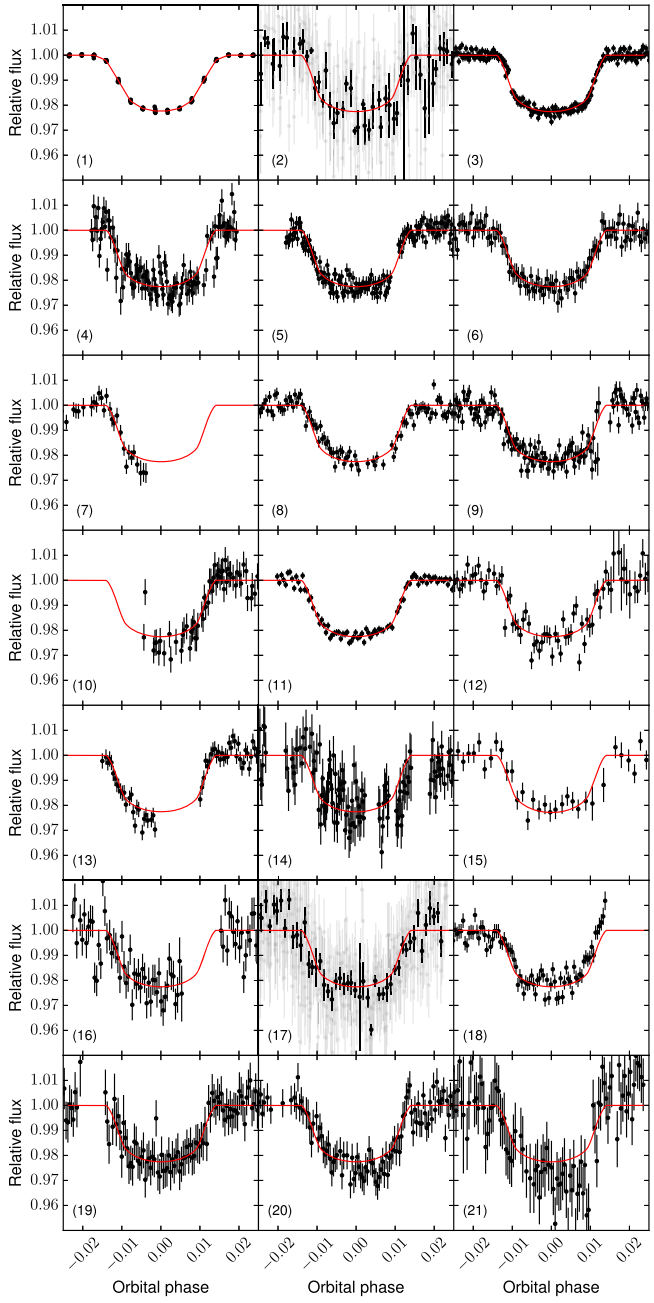

Figure 3. Phase-folded transit light curves of the transit planet K2-29 b. Panel 1 is the *K2* data, panel 2 displays the Super-WASP data, and panels 3–21 are from the ground-based facilities listed in Table 2. The red line is the best model found in the MCMC analysis. For panels 2 and 17, the gray dots are the raw data and the black dots are the same data binned to 0.001 in phase.

We ran 20 chains of 3×10^5 iteration each started randomly from the joint prior distribution. We analyzed the chains as previously and found that the planet is aligned relative to the stellar spin with a value of $\lambda = 1\overset{\circ}{.}5 \pm 8\overset{\circ}{.}7$. The derived $v \sin i_\star$ is $3.7 \pm 0.5\,\mathrm{km\,s^{-1}}$. The HARPS-N and SOPHIE data are displayed in Figure 5 together with the best-fit model.

3.4. Blend Sanity Checks

The detection of both the reflex motion and the Rossiter–McLaughlin effect is not enough to firmly assess the planetary nature of a candidate (e.g., Santos et al. 2002; Torres et al. 2005; A. Santerne et al. 2016, in preparation). The radial velocity variation is detected on star A, thus we can exclude star B from being the transit host. Even if it is quite unlikely, the system might still be a triple system located within the detection limits of AstraLux. According to Santerne et al. (2015), this triple system would imprint a significant variation in the bisector and/or FHWM.

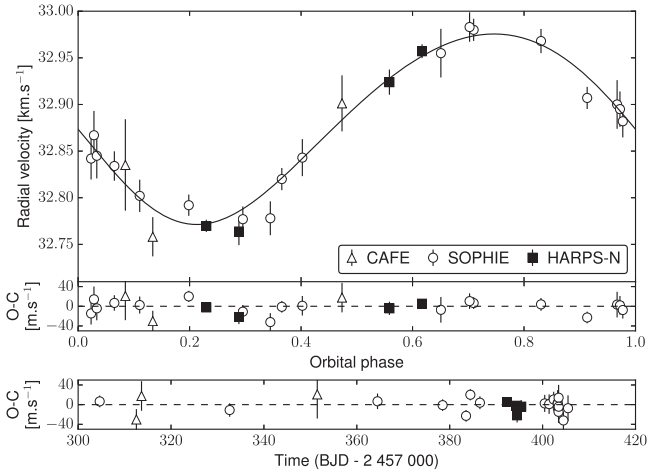

Figure 4. Phase-folded radial velocities of the exoplanet K2-29 b. The black line is the best model found and the bottom panels are the corresponding residuals, in orbital phase (middle) and in time (bottom).

We find no variation in the bisector with rms of $20\,\mathrm{m\,s^{-1}}$, $42\,\mathrm{m\,s^{-1}}$, and $15\,\mathrm{m\,s^{-1}}$ on SOPHIE, HARPS-N, and CAFE, respectively, which is compatible with the uncertainties (see Table 3). The FWHM has rms of $73\,\mathrm{m\,s^{-1}}$, $63\,\mathrm{m\,s^{-1}}$, and $50\,\mathrm{m\,s^{-1}}$ (respectively). This is larger than the typical uncertainties (see Table 3). This variability is, however, not correlated with the observed radial velocity variation. We concluded that this FWHM scatter is caused by the variability of the star highlighted in the *K2* light curve (see Figure 1).

We also derived the radial velocity amplitude for each instrument. As explained in Santerne et al. (2015), the difference of spectral resolution between SOPHIE ($R \approx 40{,}000$), CAFE ($R \approx 63{,}000$), and HARPS-N ($R \approx 110{,}000$) should lead to different radial velocity amplitudes in the case of a blend. We find that $K_{\mathrm{SOPHIE}} = 99.4 \pm 6.1\,\mathrm{m\,s^{-1}}$, $K_{\mathrm{CAFE}} = 260^{+240}_{-150}\,\mathrm{m\,s^{-1}}$, and $K_{\mathrm{HARPS-N}} = 120^{+45}_{-19}\,\mathrm{m\,s^{-1}}$. The three values are compatible within 1σ.

Finally, we reduced the SOPHIE and HARPS-N data using a binary mask corresponding to a K5 dwarf. Even if this mask does not correspond to the spectral type of the host star, it might reveal the presence of an unresolved colder stellar companion (Santerne et al. 2015). The radial velocity amplitude derived with the K5V mask is consistent within the uncertainties with the one derived with a G2V mask.

From the absence of evidence of a blend in the spectroscopic and high-resolution imaging, we conclude that this candidate is a *bona-fide* planet.

3.5. The Planetary System

Based on the results of the combined and Rossiter–McLaughlin analyses, we derived the physical parameters for the K2-29 system and present the results in Table 5.

The host star has a mass of $0.94 \pm 0.02\,M_\odot$ and a radius of $0.86 \pm 0.01\,R_\odot$. The age derived using the Dartmouth stellar

Table 5
Physical Parameters of the K2-29 System

Parameter	Value and Uncertainty
Orbital parameters	
Period P (day)	$3.2588321 \pm 1.9 \times 10^{-6}$
Transit epoch T_0 (BJD—2.45 × 10^6)	$3219.0095 \pm 2.2 \times 10^{-3}$
Orbital eccentricity e	0.066 ± 0.022
Argument of periastron ω (°)	132 ± 21
Inclination i (°)	$86.656^{+0.11}_{-0.08}$
Semimajor axis a (AU)	$0.04217 \pm 2.4 \times 10^{-4}$
Spin–orbit angle λ (°)	1.5 ± 8.7
Transit and Keplerian parameters	
System scale $a/R_\star$	10.51 ± 0.15
Impact parameter $b_{\rm prim}$	0.58 ± 0.02
Transit duration T_{14} (hr)	2.22 ± 0.01
Planet-to-star radius ratio k_r	$0.14188 \pm 6.2 \times 10^{-4}$
RV amplitude K (m s^{-1})	103.5 ± 5.4
Planet parameters	
Planet mass M_p ($M_{2\mathrm{J}}$)	0.73 ± 0.04
Planet radius R_p ($R_{2\mathrm{J}}$)	1.19 ± 0.02
Planet density ρ_p (g cm^{-3})	0.53 ± 0.04
Equilibrium temperature $T_{\rm eq}$ (K)	1171 ± 10
Stellar parameters	
Stellar mass $M_\star$ ($M_\odot$)	0.94 ± 0.02
Stellar radius $R_\star$ ($R_\odot$)	0.86 ± 0.01
Stellar age[a] τ (Gyr)	2.6 ± 1.2
Stellar age[b] τ (Gyr)	0.45 ± 0.25
Distance d (pc)	185 ± 3
Reddening $E(B-V)$ (mag)	0.19 ± 0.02
Systemic RV υ_0 (km s^{-1})	32.8786 ± 0.0044
Effective temperature $T_{\rm eff}$ (K)	5358 ± 38
Surface gravity log g (g cm^{-2})	4.540 ± 0.012
Iron abundance [Fe/H] (dex)	0.16 ± 0.03
Rotational velocity $\upsilon \sin i_\star$ (km s^{-1})	3.7 ± 0.5
Rotation period $P_{\rm rot}$ (day)	10.79 ± 0.02
Spectral type	G7V

Notes. All the uncertainties provided here are only the statistical ones. Errors on the models are not considered, as they are unknown. Stellar parameters are derived from the combined analysis of the data and not from the spectral analysis. We assumed $1\,R_\odot = 695{,}508$ km, $1\,M_\odot = 1.98842 \times 10^{30}$ kg, $1\,R_{2\mathrm{J}} = 71{,}492$ km, $1\,M_{2\mathrm{J}} = 1.89852 \times 10^{27}$ kg, and 1 AUau = 149,597,870.7 km.
[a] Based on the Dartmouth stellar evolution tracks.
[b] Based on lithium abundance and stellar rotation.

tracks (Dotter et al. 2008) indicates that the system is 2.6 ± 1.2 Gyr old. The age can, however, be estimated as 450 ± 200 Myr based on both A(Li) and $P_{\rm rot}$. Both values correspond to an age older than the M34 cluster (250 Myr). The star might be younger than the Hyades cluster (or Praesepe) but few members of this 625 Myr association display either lithium abundances or rotations similar to our estimates (Barrado y Navascues & Stauffer 1996; Jones et al. 1997; James et al. 2010; Barnes et al. 2015). We cannot use the activity index measured in the Ca II lines as the signal-to-noise at these wavelengths is at the order of unity and thus too low for reliable measurements. A combined analysis of both stellar and planet models as done in Guillot & Havel (2011) could provide further constraints on the age of this system.

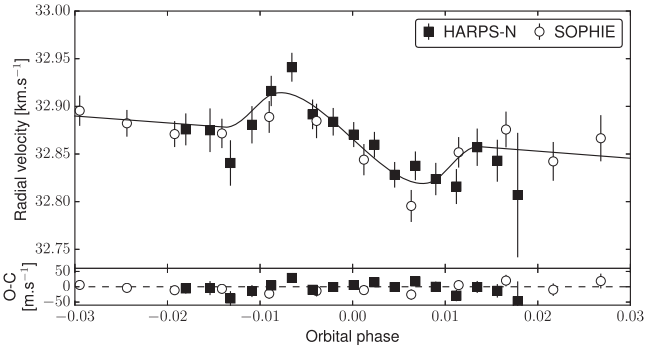

Figure 5. Observation of the Rossiter–McLaughlin effect for the planet K2-29 b. The black line is the best model found and the bottom panel is the corresponding residuals.

Several theoretical works have shown, however, that episodic accretion in the early ages can destroy lithium (Baraffe & Chabrier 2010) as well as the accretion of planetary material to fingering convection (Théado & Vauclair 2012). Considering these effects would give an even younger age for this system. Depending on the rotational evolution this star has experienced, the lithium depletion could be stronger or weaker, hence increasing the uncertainty on the age of this system.

The system is located at 185 ± 3 pc. With a separation of ∼4.″3, the stellar companion (star B) has a current sky-projected separation of about 800 AU.

We find that the transiting planet has a mass of 0.73 ± 0.04 $M_{2\mathrm{J}}$ and a radius of 1.19 ± 0.02 $R_{2\mathrm{J}}$. This gives a bulk density of 0.53 ± 0.04 g cm^{-3}. K2-29 b is therefore an inflated hot Jupiter. The orbit of the planet shows a 3σ detection of an eccentricity of 0.066 ± 0.022, but this might be caused by the effects of the stellar variability, clearly seen in the *K2* light curve, affecting the radial velocity measurements. We find a sky-projected spin–orbit angle of 1.°5 ± 8.°7. With a stellar radius of 0.86 ± 0.01 $R_\odot$ and a rotational period of 10.79 ± 0.02 days, the rotational velocity of the star is 4.06 ± 0.05 km s^{-1}, which is consistent with the $\upsilon \sin i_\star$ measured with the Rossiter–McLaughlin effect of 3.7 ± 0.5 km s^{-1}. The star is therefore seen nearly equator-on and the transiting planet is well aligned with the stellar spin. With a central star $T_{\rm eff} < 6250$ K, this aligned system is in agreement with the other systems of this kind reported in Albrecht et al. (2012).

4. CONCLUSION AND DISCUSSION

In this paper, we report the discovery of a new hot Jupiter co-discovered in the *K2* and archival Super-WASP data. The host star is the primary of a visual binary system.

The star K2-29 was observed during *K2*'s campaign 4, which also targeted both the Pleiades and the Hyades clusters. It is unlikely that this system belongs to Pleiades (membership probability of less than 2%) as estimated by Bouy et al. 2015, in agreement with Sarro et al. (2014). Interestingly, we note that the system has lithium (for this stellar temperature) and iron abundances that are compatible with the Hyades. Moreover, the systemic radial velocity of the star also agrees with the Hyades (Perryman et al. 1998). However the system is too far away and the proper motion is not compatible with this cluster. We conclude it is unlikely that it belongs to the Hyades. Using the proper motion listed in Table 1, we find that the system has galactic velocities of $U = -17$ km s^{-1}, $V = 11$ km s^{-1}, and $W = -23$ km s^{-1}, and thus has a 99%

probability of belonging to the thin disk. This new hot Jupiter has also been reported in Johnson et al. (2016).

K2-29 is an inflated hot Jupiter amenable for precise spectrophotometric characterization of its atmosphere. Assuming an H_2 dominated atmosphere the planet gravity and equilibrium temperature would imply a scale height equal to about 418 km. The corresponding photometric precision on the transit depth measurement ($\sim\frac{2R_pH}{R_*^2}$) is ∼190 ppm. Such a precision can be achieved using, for example, ground-based differential spectrophotometry, given that the presence of a close-by companion will allow optimal control of systematics and subtraction of the Earth atmosphere. On a 4 m class telescope, considering the effect of atmospheric scintillation and assuming an optimized observing strategy ($t_{\rm exp} \sim 15$ s), for one single transit event we expect to achieve a precision of around half the scale height on this target.

The two stars (target and companion) have a more favorable brightness contrast in the near-infrared ($Ks_A \sim 10.1$, $Ks_B \sim 10.9$). This means that K2-29 should be well suited for analysis in the near-infrared domain, in particular from space with the *James Webb Space Telescope* (Greene et al. 2015) or *ARIEL* (Tinetti 2015). In particular, the 1.4 μm water absorption band has been found to be a powerful tracer of exoplanet atmospheric chemistry (Sing et al. 2016). The strength of this absorption band appears to be related to the presence or absence of clouds and hazes in the atmosphere, as probed, for instance, by optical observations. Clear atmospheric models would imply a 1.4 μm absorption depth equal to about four scale heights (e.g., Hubbard et al. 2001). The equilibrium temperature of this exoplanet implies, however, that several compounds, in particular silicates, should be sequestered in the bottom atmosphere in the form of condensates (Burrows & Sharp 1999) and could potentially form cloud layers which can partially or totally mask the absorption features depending on the altitude at which they are found.

We thank the anonymous referee for his/her fruitful comments and Ph. Rousselot for the share of nights with HARPS-N. The Porto group acknowledges the support from the Fundação para a Ciência e Tecnologia, FCT (Portugal) in the form of the grants, projects, and contracts UID/FIS/04434/2013 (POCI-01-0145-FEDER-007672), PTDC/CTE-AST/098528/2008, PTDC/FIS-AST/1526/2014, SFRH/BPD/76606/2011, SFRH/BPD/70574/2010, SFRH/BDP/71230/2010, IF/00169/2012, IF/00028/2014, IF/01312/2014, and POPH/FSE (EC) by FEDER funding through the program "Programa Operacional de Factores de Competitividade—COMPETE." A.S. is supported by the European Union under a Marie Curie Intra-European Fellowship for Career Development with reference FP7-PEOPLE-2013-IEF, number 627202. J.L.-B. acknowledges financial support from the Marie Curie Actions of the European Commission (FP7-COFUND) and the Spanish grant AYA2012-38897-C02-01. J.M.A. acknowledges funding from the European Research Council under the ERC Grant Agreement n. 337591-ExTrA. D.J.A. and D.P. acknowledge funding from the European Union Seventh Framework programme (FP7/2007–2013) under grant agreement No. 313014 (ETAEARTH). O.D. acknowledges support by CNES through contract 567133. P.A.W. acknowledges the support of the French Agence Nationale de la Recherche (ANR), under program ANR-12-BS05-0012 "Exo-Atmos."

This work is partly based on observations made with the Italian Telescopio Nazionale Galileo (TNG) operated on the island of La Palma by the Fundacin Galileo Galilei of the INAF (Istituto Nazionale di Astrofisica) at the Spanish Observatorio del Roque de los Muchachos of the Instituto de Astrofisica de Canarias. This work is partly based on observations made at Observatoire de Haute-Provence (CNRS), France. This work is partly based on observations collected at the Centro Astronmico Hispano Alemn (CAHA) at Calar Alto, operated jointly by the Max-Planck Institut für Astronomie and the Instituto de Astrofsica de Andaluca (CSIC).

This work makes use of observations from the LCOGT network. This research has made use of the VizieR catalogue access tool, CDS, Strasbourg, France. The original description of the VizieR service was published in A&AS 143, 23. This research has made use of the NASA Exoplanet Archive, which is operated by the California Institute of Technology, under contract with the National Aeronautics and Space Administration under the Exoplanet Exploration Program. This research was made possible through the use of the AAVSO Photometric All-Sky Survey (APASS), funded by the Robert Martin Ayers Sciences Fund. This publication makes use of data products from the Wide-field Infrared Survey Explorer, which is a joint project of the University of California, Los Angeles, and the Jet Propulsion Laboratory/California Institute of Technology, funded by the National Aeronautics and Space Administration. This publication makes use of data products from the Two Micron All-Sky Survey, which is a joint project of the University of Massachusetts and the Infrared Processing and Analysis Center/California Institute of Technology, funded by the National Aeronautics and Space Administration and the National Science Foundation.

Facilities: *Kepler* (K2), TNG (HARPS-N), OHP (SOPHIE), CAO:2.2m, Super-WASP.

REFERENCES

Aceituno, J., Sánchez, S. F., Grupp, F., et al. 2013, A&A, 552, A31
Ahn, C. P., Alexandroff, R., Allende Prieto, C., et al. 2012, ApJS, 203, 21
Albrecht, S., Winn, J. N., Johnson, J. A., et al. 2012, ApJ, 757, 18
Allard, F. 2014, in IAU Symp. 299, Exploring the Formation and Evolution of Planetary Systems (Cambridge: Cambridge Univ. Press), 271
Almenara, J. M., Astudillo-Defru, N., Bonfils, X., et al. 2015, A&A, 581, L7
Armstrong, D. J., Kirk, J., Lam, K. W. F., et al. 2015a, A&A, 579, A19
Armstrong, D. J., Santerne, A., Veras, D., et al. 2015b, A&A, 582, A33
Baglin, A., Auvergne, M., Boisnard, L., et al. 2006, in 36th COSPAR Scientific Assembly 36, 3749
Baraffe, I., & Chabrier, G. 2010, A&A, 521, A44
Baranne, A., Queloz, D., Mayor, M., et al. 1996, A&AS, 119, 373
Barnes, S. A., Weingrill, J., Granzer, T., Spada, F., & Strassmeier, K. G. 2015, A&A, 583, A73
Barrado y Navascues, D., & Stauffer, J. R. 1996, A&A, 310, 879
Barros, S. C. C., Almenara, J. M., Demangeon, O., et al. 2015, MNRAS, 454, 4267
Boisse, I., Eggenberger, A., Santos, N. C., et al. 2010, A&A, 523, A88
Borucki, W. J., Koch, D., Jenkins, J., et al. 2009, Sci, 325, 709
Bouchy, F., Díaz, R. F., Hébrard, G., et al. 2013, A&A, 549, A49
Bouchy, F., Isambert, J., Lovis, C., et al. 2009, EAS Publications Series, 37, 247
Boué, G., Montalto, M., Boisse, I., Oshagh, M., & Santos, N. C. 2013, A&A, 550, A53
Bouy, H., Bertin, E., Sarro, L. M., et al. 2015, A&A, 577, A148
Brown, T. M., Baliber, N., Bianco, F. B., et al. 2013, PASP, 125, 1031
Burrows, A., & Sharp, C. M. 1999, ApJ, 512, 843
Claret, A., & Bloemen, S. 2011, A&A, 529, A75
Collins, K. A., Kielkopf, J. F., & Stassun, K. G. 2016, arXiv:1601.02622
Cosentino, R., Lovis, C., Pepe, F., et al. 2012, Proc. SPIE, 8446, 84461V

Cox, A. N. 2000, Allen's Astrophysical Quantities (4th ed.: New York: Springer)
Croll, B., Albert, L., Jayawardhana, R., et al. 2015, ApJ, 802, 28
Crossfield, I. J. M., Petigura, E., Schlieder, J. E., et al. 2015, ApJ, 804, 10
Cutri, R. M., Wright, E. L., Conrow, T., et al. 2013, yCat, 2328
Díaz, R. F., Almenara, J. M., Santerne, A., et al. 2014, MNRAS, 441, 983
Dotter, A., Chaboyer, B., Jevremović, D., et al. 2008, ApJS, 178, 89
Eastman, J., Siverd, R., & Gaudi, B. S. 2010, PASP, 122, 935
Fedorov, P. N., Akhmetov, V. S., & Bobylev, V. V. 2011, MNRAS, 416, 403
Greene, T. P., Line, M. R., Montero, C., et al. 2015, arXiv:1511.05528
Guillot, T., & Havel, M. 2011, A&A, 527, A20
Høg, E., Fabricius, C., Makarov, V. V., et al. 2000, A&A, 355, L27
Hormuth, F., Hippler, S., Brandner, W., Wagner, K., & Henning, T. 2008, Proc. SPIE, 7014, 701448
Howell, S. B., Sobeck, C., Haas, M., et al. 2014, PASP, 126, 398
Hroch, F. 2014, Astrophysics Source Code Library, ascl:1402.006
Hubbard, W. B., Fortney, J. J., Lunine, J. I., et al. 2001, ApJ, 560, 413
Huber, D., Bryson, S. T., Haas, M. R., et al. 2015, arXiv:1512.02643
James, D. J., Barnes, S. A., Meibom, S., et al. 2010, A&A, 515, A100
Johnson, M. C., Gandolfi, D., Fridlund, M., et al. 2016, AJ, 151, 171
Jones, B. F., Fischer, D., Shetrone, M., & Soderblom, D. R. 1997, AJ, 114, 352
Kipping, D. M. 2010, MNRAS, 408, 1758
Kipping, D. M. 2013, MNRAS, 434, L51
Lillo-Box, J., Barrado, D., & Bouy, H. 2014, A&A, 566, A103
Lillo-Box, J., Barrado, D., Santos, N. C., et al. 2015, A&A, 577, A105
McQuillan, A., Mazeh, T., & Aigrain, S. 2013, ApJL, 775, L11
McQuillan, A., Mazeh, T., & Aigrain, S. 2014, ApJS, 211, 24
Mortier, A., Sousa, S. G., Adibekyan, V. Z., Brandão, I. M., & Santos, N. C. 2014, A&A, 572, A95
Munari, U., Henden, A., Frigo, A., et al. 2014, AJ, 148, 81
Pepe, F., Mayor, M., Galland, F., et al. 2002, A&A, 388, 632
Perryman, M. A. C., Brown, A. G. A., Lebreton, Y., et al. 1998, A&A, 331, 81
Pollacco, D. L., Skillen, I., Collier Cameron, A., et al. 2006, PASP, 118, 1407
Santerne, A., Díaz, R. F., Almenara, J.-M., et al. 2015, MNRAS, 451, 2337
Santerne, A., Díaz, R. F., Moutou, C., et al. 2012, A&A, 545, A76
Santerne, A., Hébrard, G., Deleuil, M., et al. 2014, A&A, 571, A37
Santerne, A., Moutou, C., Tsantaki, M., et al. 2016, A&A, 587, A64
Santos, N. C., Mayor, M., Naef, D., et al. 2002, A&A, 392, 215
Santos, N. C., Sousa, S. G., Mortier, A., et al. 2013, A&A, 556, A150
Sarro, L. M., Bouy, H., Berihuete, A., et al. 2014, A&A, 563, A45
Sing, D. K., Fortney, J. J., Nikolov, N., et al. 2016, Natur, 529, 59
Sousa, S. G. 2014, arXiv:1407.5817
Sousa, S. G., Santos, N. C., Adibekyan, V., Delgado-Mena, E., & Israelian, G. 2015, A&A, 577, A67
Sousa, S. G., Santos, N. C., Israelian, G., Mayor, M., & Udry, S. 2011, A&A, 533, A141
Southworth, J. 2011, MNRAS, 417, 2166
Stevenson, K. B., Désert, J.-M., Line, M. R., et al. 2014, Sci, 346, 838
Strehl, K. 1902, AN, 158, 89
Théado, S., & Vauclair, S. 2012, ApJ, 744, 123
Tinetti, G. 2015, in AAS/Division for Planetary Sciences Meeting Abstracts 47, 416.20
Torres, G., Konacki, M., Sasselov, D. D., & Jha, S. 2005, ApJ, 619, 558